MATERIAL MODELLING AND SIMULATION OF 3D CONCRETE PRINTING PROCESS

JIŘÍ RYMEŠ[*], JAN ČERVENKA[*], AND LIBOR JENDELE[*]

[*] Červenka Consulting
Na Hřebenkách 2667/55, 150 00 Prague, Czech Republic
e-mail: jiri.rymes@cervenka.cz, www.cervenka.cz

Key words: Non-linear modelling, Additive manufacturing, 3D concrete printing (3DCP), Kinetic material model

Abstract: 3D concrete printing (3DCP) is an innovative construction technology with the potential to revolutionize the concrete industry. As the research and development of 3DCP accelerate, there is a growing need for suitable numerical tools for the simulation of the process. In response to this need, this paper presents an integrated approach, combining a time-dependent material model for hardening concrete with a finite element method (FEM) solver, capable of progressively activating finite elements along the printing trajectory. The time-dependent material model is derived directly from the underlying hydration mechanism thus allowing consideration of temperature impact on the development of mechanical properties. The FEM solver is formulated to account for second-order effects. To demonstrate the applicability of the proposed framework, an example simulating layer-by-layer construction of a real pilot house is shown.

1 INTRODUCTION

Utilizing the additive manufacturing process represented a breakthrough in engineering practice. The otherwise costly and laborious prototyping process traditionally done by hand-craft modelling or injection moulding was reduced to a fraction of cost and time. Furthermore, the 3D printing allows for great customisation of the products or even reduces the production cost for products with low repeatability. Aided by modern and user-friendly CAD software, the production of 3D-printed products is now available to a much broader creator base than just a narrow spectrum of specially trained engineers.

Recently, additive manufacturing has been adopted also in the concrete industry, where referred to as 3D concrete printing (3DCP). Among its benefits is the optimization of material usage and lowering labour demands while allowing for the execution of ambitious architectonical designs without the need for additional formwork.

Nowadays, the 3DCP technology is rapidly expanding. The review of the state of the 3DCP technology published by Ma et al. [1] showed that before 2016, less than 40 scientific papers in total were published on the topic of 3DCP. In 2021, the total number of journal publications already exceeded 400. The authors documented a similar sharp increase in the number of approved patents and 3DCP projects, which illustrates that the interest in this technology is not limited only to the scientific community, but it is promising also from the perspective of the industry sector.

As the 3DCP technology rapidly develops, there is a need for suitable numerical tools for the simulation of the process. Compared to additive manufacturing employing polymer materials, specific issues arise when it comes to 3DCP. This study discusses some specific

aspects related to the numerical simulation of the additive manufacturing process and proposes a simulation framework composed of a time-dependent non-linear material model and finite element method solver, which can simulate the additive manufacturing process. This framework has been implemented in the ATENA software package and its applicability is demonstrated using an example of an actual pilot building structure constructed by 3DCP.

2 NON-LINEAR SIMULATION FOR ADDITIVE MANUFACTURING

The finite element method (FEM) is routinely applied during the designing of reinforced concrete structures. Mostly, for obtaining internal forces, which are subsequently used for dimensioning critical cross-sections. Similarly, FEM can be used to assess the performance of 3D-printed structures, including the construction phase when the material is still fresh. The general applicability of the non-linear FEM simulation of 3DCP has been shown for small-scale laboratory experiments [2] and, in this study, we further improve the material modelling by implementing a hydration model that governs the development of material properties in time.

2.1 Fracture-plastic material model

Apart from the linear FEM, also the non-linear FEM has been adopted in the design of new and assessment of existing structures in recent years. By introducing non-linear relationships in material laws, a realistic response of the finite element model to applied loads can be obtained. For reinforced concrete material, the non-linear material behaviour refers for instance to the cracking of concrete when its tensile strength is exceeded, crushing when subjected to excessive compressive stresses, and, for steel reinforcement, yielding or even rupturing.

In the model of Červenka et al. [3,4], the development of tensile cracks is simulated using the smeared crack approach with a crack band when the softening is controlled by the amount of dissipated fracture energy as shown in Figure 1.
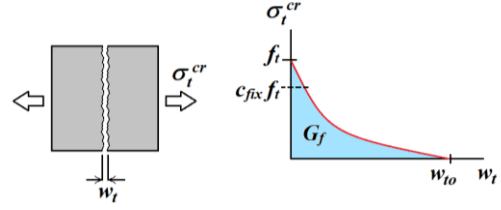

Figure 1: The softening law controlled by the amount dissipated fracture energy, which is adopted in tension for simulation of crack opening.

The fracture energy approach in tension is combined with the plasticity approach with Menetrey & Willam failure criterion [5] shown in Figure 2 and used in the compression branch. The reinforcement bars can be either discrete or smeared, both allowing the prescription of a multilinear stress-strain relationship.
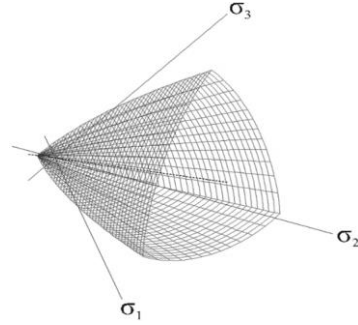

Figure 2: Menetrey & Willam failure criterion used in the compression branch of the non-linear material model [5].

2.2 Element activation and loads

In non-linear FEM, the loads are typically gradually increased to a prescribed load level in several load steps. The reason is that once the linear material behaviour is exceeded, the material non-linearities, for instance in the form of concrete cracks, accurately localize in the model during the simulation. This somehow corresponds to a realistic static loading since, as the applied load is gradually increased, any potential local damage causes a redistribution of the overall flow of internal forces.

For the simulation of additive manufacturing, each load step corresponds to the given time of the printing. In the approach presented in this study, before the simulation starts, an element's construction time is prescribed for each finite element in the model. This element's construction time corresponds

to the time when the given part of the structure is printed. Then, as the solution runs, the finite elements are gradually activated. The element's construction time is the key variable used not only for determining the solution step when the element is activated but also for governing the loads and material model parameters. It is calculated directly from the trajectory of the printing nozzle. The trajectory is either given manually or can be directly extracted from the G-code file produced by the slicer. On top of that, for certain parts of the model constructed independently, the element's construction time can be explicitly specified. This is typically the case for reinforcement elements or lintels.

Once the element is activated in the simulation, it is loaded by its self-weight. In other words, only the finite element with construction time $t_{constr} \leq t$, where t stands for the time at the current solution step, are loaded by the self-weight body loads. For the time-dependent laws such as shrinkage, the load is introduced gradually for each finite element thus the shrinkage load differs over the model. For the shrinkage prescribed by an arbitrary function $\varepsilon(t)$, the applied initial strains at a given element can be written as:

$$\varepsilon_x = \varepsilon_y = \varepsilon_z = \varepsilon\left(t - t_{constr}\right) \quad . \qquad (1)$$

Apart from self-weight and shrinkage loads, other loads can be used in the simulation such as surface loads simulating wind actions.

2.3 Kinetic material model

The ability of a material model to accurately describe the actual material behaviour is crucial for numerical simulations. In the case of 3DCP, the material model must be also able to simulate the gradual increase of the material performance characteristic as the material changes its state from thixotropic, non-Newtonian fluid into solid hardened paste [6]. This study adopts the model of Červenka et al. [3,4] implemented in the ATENA software package [7] and presents its time-dependent component for the simulation of the hardening paste used for 3D concrete printing.

Ideally, the definition of material parameters should cover the material age from

the moment of printing up to the time of decades, thus allowing complex assessment in a single FEM analysis. During this period, the material performance characteristics are governed by two mechanisms. Just after deposition of the material, its initial strength is given by the thixotropic nature of the paste. This stage can be further divided into the re-flocculation phase controlled by the re-creation of the inter-particle bonds and the structuration phase [6,8], when the static yield stress increases due to the formation of early hydration products. These mechanisms are responsible for the material performance until the end of the cement dormant period, typically at least for the first couple of hours. Once the cement dormant period ends, the reaction rate sharply increases and the formation of cement hydrates, mainly the calcium-silicate-hydrates, hardens the material.

In this study, the gradual improvement of the material performance characteristics is simulated by changing the parameters of the fracture-plastic model. In this approach, each integration point in the model has different material parameters, which are updated at each solution step to simulate the hardening of the paste. We have developed an approach how to deduce the time evolution of the parameters for the fracture-plastic material model described previously. The proposed approach is composed of three steps:
1) Computing of the hydration kinetics,
2) Calculation of the development of compressive strength based on the degree of hydration (DoH),
3) Calculate the parameters of the material model based on the compressive strength value.

In the first step, the hydration kinetics can be either inputted manually based on direct measurement of the DoH or can be obtained using the affinity hydration model [9] in the form:

$$\frac{\partial \alpha}{\partial t} = B_1\left(\frac{B_2}{\alpha_\infty} + \alpha\right)\left(\alpha_\infty - \alpha\right)\exp\left[-\bar{\eta}\frac{\alpha}{\alpha_\infty}\right] , \quad (2)$$

where α is the DoH, α_∞ is the maximum DoH, and B_1, B_2, and $\bar{\eta}$ are the parameters of the
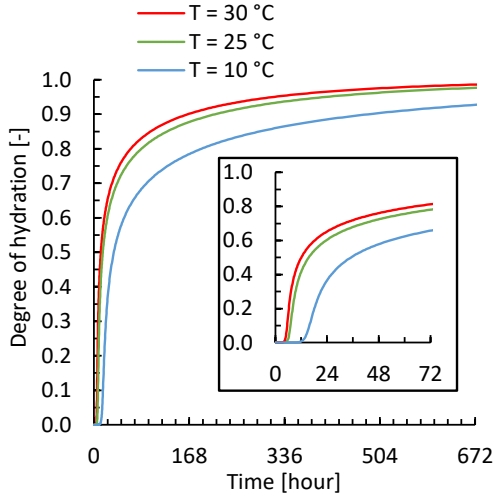
Figure 3: Example of the hydration curve defining the increase of the degree of hydration in time (the detail showing the first 72 hours).

Figure 4: Example of a function relating the degree of hydration and relative compressive strength.

hydration model describing its kinetics.

Since the development of the material properties is based on the hydration process, it can easily account for different temperature conditions using basic relationships of the physical chemistry. The Arrhenius equation gives the relationship between the rate of reaction at a given temperature T and reference temperature T_{ref}. It can be used for adjusting the hydration rate as follows:

$$\frac{\partial \alpha_T}{\partial t} = \frac{\partial \alpha}{\partial t} k_T = \frac{\partial \alpha}{\partial t} \exp\left[\frac{E_a}{R}\left(\frac{1}{T_{ref}} - \frac{1}{T}\right)\right] , \quad (3)$$

where k_T is the rate constant, E_a is the activation energy, and R is the universal gas constant. Using this relationship, the development of material performance can be easily scaled to account for the external temperature at the time of printing. An example of the development of DoH in time is shown in Figure 3. For the sake of comparison, three curves corresponding to different temperatures are plotted.

In the second step, based on the development of the DoH in time, the gain of relative compressive strength in time is computed using a constitutive relationship. At this stage of calculation, the different mechanisms governing the strength increase before and after the dormant period are considered. During the dormant period, when the rate of hydration is slow, the gain of the relative compressive
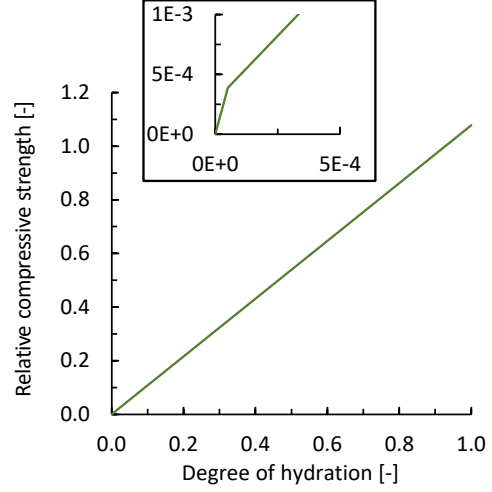
strength with respect to the DoH is rapid to account for the structuration of the fresh paste. Once the dormant period ends, the rate of the relative compressive strength gain becomes approximately proportional to the rate of hydration. An example of the function relating the relative compressive strength to the DoH is plotted in Figure 4. To account for the static yield stress of the freshly printed paste, the relative compressive strength can have a non-zero value at $\alpha = 0$. Next, the relative compressive strength is scaled using the compressive strength given at an arbitrary time.

In the third step, the remaining material

Table 1: Summary of the relations for generation of the parameters of the fracture-plastic model.

Parameter: symbol [unit]	Formula
Compression strength: f_c [MPa]	$f_c(\alpha)$
Young's modulus: E [MPa]	$\left(6000 - 15.5 f_{c,28}\right)\sqrt{f_c}$
Tensile strength: f_t [MPa]	$0.3 f_c^{\frac{2}{3}}$
Specific fracture energy: G_f [N/m]	$73 f_c^{0.18}$
Critical compressive displacement: w_d [mm]	-0.5
Onset of non-linearity in compression: f_{c0} [MPa]	$\frac{2}{3} f_c$
Plastic strain at compressive strength: ε_{cp} [MPa]	f_c / E_{28}

4

Figure 5: The Prvok House on the Vltava River in the city centre of Prague, Czech Republic (courtesy of Scoolpt s.r.o.).

parameters for the definition of the fracture-plastic material model are computed using a set of constitutive laws. These relations are summarised in Table 1.

2.4 Simulation of the loss of stability

The numerical simulation of additive manufacturing should be able to capture the loss of stability of the structural element under printing. As the height of the printed element increases, the fresh paste in the bottom layers transfers the weight of the layers above while having low material performance, mainly the yield stress. Due to this, the deflection of the structure increases and may lead to progressive buckling collapse, which is a typical failure mechanism for this construction technology.

To simulate this second-order effect, the solution method presented in this study uses the updated Lagrangian formulation, where the finite element mesh deforms with the structure. Therefore, during the step-by-step solution, the nodal coordinates are updated, and the solution of the next step is always based on the deformed geometry obtained in the previous step. Furthermore, the solid finite elements support geometrical non-linearity. This allows for capturing the second-order effects and simulation of the progressive buckling.

3 APPLICATION EXAMPLE

3.1 Introduction of the Prvok House

The simulation framework described in the previous chapter has been applied to simulate the construction process of the Prvok House, produced in Prague, Czech Republic. The photo of the house after the construction is shown in Figure 5. The term Prvok, in English translation Protozoan, signifies not only the first application of 3DCP on a structural scale in the Czech Republic but also refers to the design resembling the shape of the very first animal species.

The structure of the Prvok house is composed of sandwich walls with outer and inner surfaces being connected with stirrup reinforcement. The thickness of one layer is approximately 45 mm and the height is approximately 12 mm. The wavy-like geometry of the outer wall provides Prvok with its unique architectural look while ensuring better out-of-plane stability. The inner part of the sandwich wall does not have the wavy-like geometry, but its stability is improved by sigma-shaped columns with a spacing of approximately 0.5 m.

3.2 Model and material properties

The Prvok House was constructed using a commercial ready-to-use fibre-reinforced concrete mixture specifically developed for 3DCP. Based on the data provided by the producer in the technical specification, the parameters of the kinetic material model were
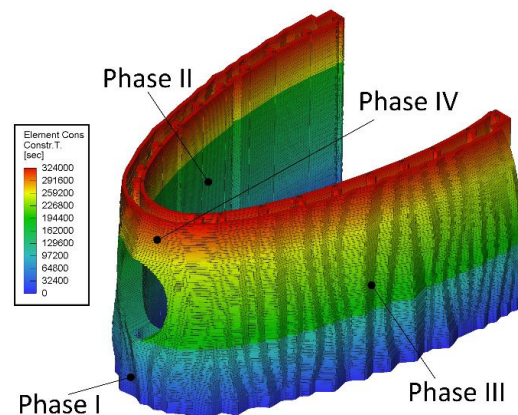

Figure 6: Model of the Prvok House schematically showing the construction sequence and the construction time (in seconds) of different parts of the structure.
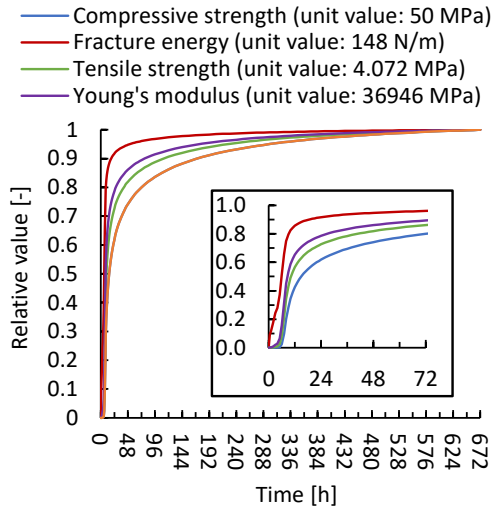
Figure 7: Relative functions showing an increase of selected parameters of the material model in time.

estimated and are shown in Figure 7. The stirrup reinforcement was not neglected in the model.

The finite element model represented one-half of the whole house, including an elliptical window in the front of the house. The printing sequence is schematically illustrated in Figure 6. First, the whole length of the wall below the window was printed. In the second phase, the wall on the left side of the window was constructed up to the height of the window followed by the part of the wall on the right. Finally, the part of the sandwich wall above the window was printed in its entire length. In the initial analysis, the total construction time was assumed approximately 90 hours. In this construction sequence and with constant printing velocity, the construction speed of the

part of the wall on the sides of the window is approximately double compared to the part of the wall below the window. Therefore, this part might be sensitive to potential collapse during printing. Some further details about this simulation can be found in our other study [10].

3.3 Results

In Figure 8, the results of the minimum principal strains are plotted just after finishing the printing process. In this plot, the areas, where the compressive plastic deformation is concentrated, are shown. Naturally, as the construction speed is doubled for the parts of the wall on both sides of the window, larger compressive plastic strain (i.e., larger plastic deformation) is predicted there by the analysis results.

The largest compressive strain is observed at the top of the opening. This results from the fact that no additional supports were applied there and the whole region was supported only by the arching effect. Due to this fact, cracks with a maximum width of 0.6 mm are predicted there as shown in Figure 9. It should be noted that these cracks originate only from the mechanical loading as all shrinkage was neglected in this analysis.

3.4 Accelerated printing

In the second analysis, the printing velocity was increased ten times to observe how it would affect the stability of the structure. By increasing the printing velocity, the material
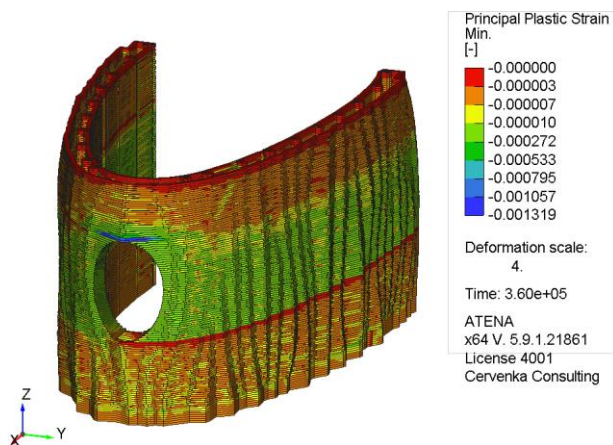

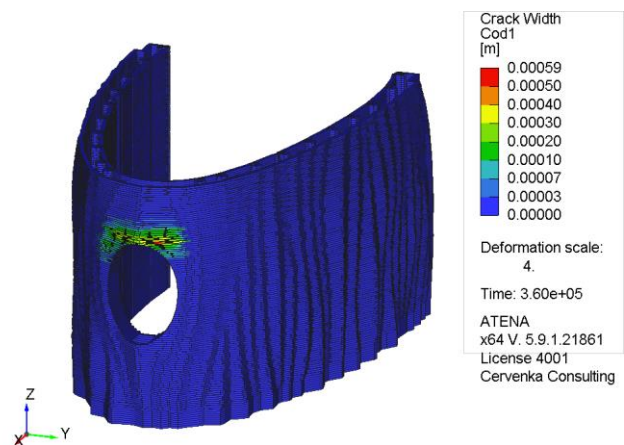**Figure 8**: Distribution of the minimum principal plastic strains over the model.

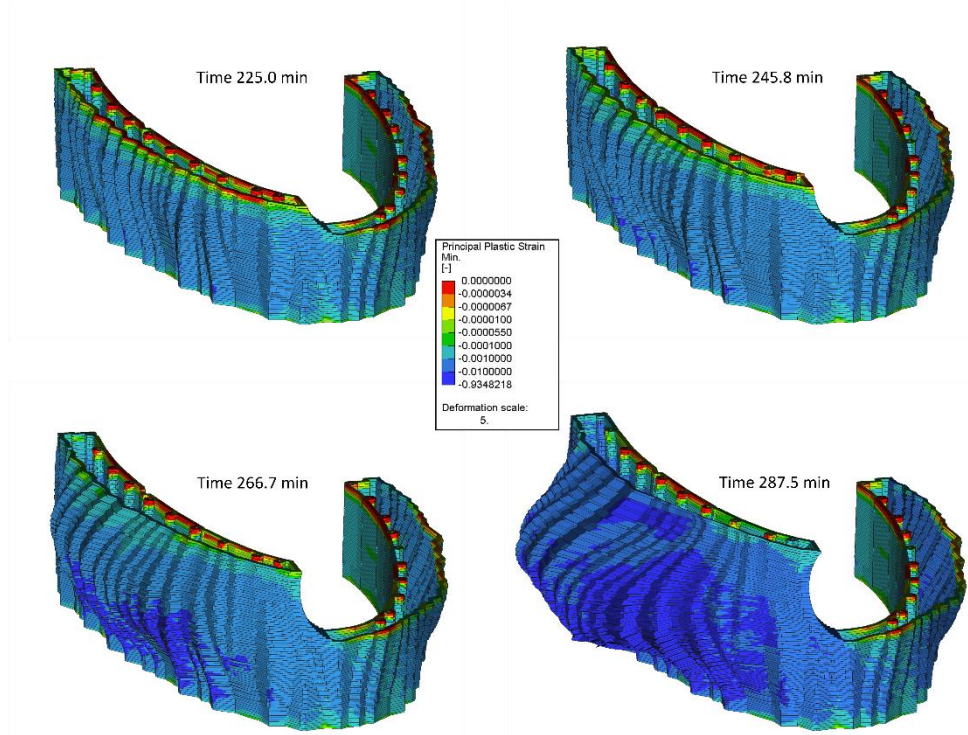**Figure 9**: Distribution of the crack width over the model.

6

Figure 10: Progressive collapse of the sandwich wall for the simulation with the printing velocity increased 10x (deformation increased 5x).

has less time to harden before the next layer is deposited on top of it.

In this case, the buckling of the wall occurred. The progressive increase in the horizontal deflection during the collapse is shown in Figure 10. As can be seen, the wall gradually buckles outward. This mechanism is enhanced since the finite elements are activated at their initial position according to the G-code during the simulation. Or, more precisely, the bottom surface of the element is connected to the nodes of the elements in the layer below while the nodes of the top surface have the coordinates defined in the G-code. This mechanism gradually shifts the resulting force of the self-weight increasing the bending moment in the sandwich wall.

5   CONCLUSIONS

This study shows the application of the non-linear finite element method in the simulation of the construction process by the 3D concrete printing technology. The proposed method utilizes a fracture-plastic material model, whose parameters develop according to the hydration kinetics thus simulating the hardening of the material. During the analysis, the finite elements are gradually activated along the printing trajectory, each having its unique element's construction time used for evaluation of the material properties at the given solution step. The formulation of the finite element method allows for consideration of geometrical non-linearities and thus is capable of capturing the loss of stability, that typically occurs at rapid printing velocities.

The presented approach has been applied to the simulation of the 3D concrete printing of the Prvok House, Czech Republic. The results predicted the regions, where plastic damage may be expected. Furthermore, it has been shown that a progressive buckling collapse may develop if the printing velocity is significantly increased.

7

REFERENCES

[1] G. Ma, R. Buswell, W.R. Leal da Silva, L. Wang, J. Xu, S.Z. Jones, Technology readiness: A global snapshot of 3D concrete printing and the frontiers for development, Cem. Concr. Res. 156 (2022) 106774. https://doi.org/10.1016/j.cemconres.2022.106774.

[2] M. Vaitová, L. Jendele, J. Červenka, Printing of Concrete Structures Modelled by FEM, Solid State Phenom. 309 (2020) 261–266.

[3] J. Červenka, V.K. Papanikolaou, Three dimensional combined fracture–plastic material model for concrete, Int. J. Plast. 24 (2008) 2192–2220. https://doi.org/10.1016/J.IJPLAS.2008.01.004.

[4] J. Červenka, V. Červenka, R. Eligehausen, Fracture-plastic material model for concrete, application to analysis of powder actuated anchors, in: Proc. Fram., 1998: pp. 1107–1116.

[5] P.M. and K.J. Willam, Triaxial Failure Criterion for Concrete and its Generalization, ACI Struct. J. 92 (n.d.). https://doi.org/10.14359/1132.

[6] V. Červenka, L. Jendele, J. Červenka, ATENA Program Documentation: Part 1 Theory, Prague, 2022.

[7] N. Roussel, A thixotropy model for fresh fluid concretes: Theory, validation and applications, Cem. Concr. Res. 36 (2006) 1797–1806. https://doi.org/10.1016/j.cemconres.2006.05.025.

[8] J. Kruger, S. Zeranka, G. van Zijl, An ab initio approach for thixotropy characterisation of (nanoparticle-infused) 3D printable concrete, Constr. Build. Mater. 224 (2019) 372–386. https://doi.org/10.1016/J.CONBUILDMAT.2019.07.078.

[9] D. Gawin, F. Pesavento, B.A. Schrefler, Hygro-thermo-chemo-mechanical modelling of concrete at early ages and beyond. Part I: hydration and hygro-thermal phenomena, Int. J. Numer. Methods Eng. 67 (2006) 299–331. https://doi.org/https://doi.org/10.1002/nme.1615.

[10] L. Jendele, J. Rymeš, J. Červenka, Optimazing digital 3D printing of concrete structures, in: Proc. 77th RILEM Annu. Week 2023, 2023.